

**POST-MASTECTOMY RADIOTHERAPY INVOLVING  
SUPRACLAVICAL NODES – MATCHLINE DOSE, TUMOUR  
DOSE AND ORGANS AT RISK DOSE**

**by**

**AHMAD SALEEM SALEM ALZOUBI**

**Thesis submitted in fulfillment of the requirements  
for the degree of  
Doctor of Philosophy**

**February 2009**

*I would like to express my heartfelt gratitude to my*

*father ...*

*may god rest his soul in peace*

*To his soul I dedicate this thesis.*

## ACKNOWLEDGMENTS

"All praises and thanks to ALLAH"

I would like to express my sincere appreciation and heartfelt thanks to my main supervisor, Professor Ahmad Shukri, my co- supervisors, Associate Professor Sivamany Kandaiya and Associate Professor Esam Elsherbieny for their creative guidance, intellectual support, stimulating discussions and inspiring words. I am grateful for their excellent hospitality and wonderful attitude.

Also, I would like to express my gratitude to School of Physics, Universiti Sains Malaysia and the Medical Physics lab assistance Yahya Ibrahim.

I am indebted to Universiti Sains Malaysia for providing me with a fellowship. My grateful to the Radiotherapy Unit of Mt Miriam Hospital in Penang, Malaysia for use of the LINAC. My thanks to the physicists at the Mt Miriam Hospital and Pantai Mutiara Hospital for all their help.

A great thanks from my heart to my mother for her prayer, unlimited support and true love had maimed the geographical distances between us. She stands by me, raised me, supported me, taught me, and loves me. To her I dedicate this thesis.

I would like to express my warmest thanks to my wonderful wife Sajedh and our children Eba'a, Lama and Abdul Rahman for their understanding, patience and support throughout the period of my research.

I would also like to thank my lovely brothers Mohammad and Ebraheem and beloved sisters Dea, Khulood, Zoha, Emteyaz and Ala'a for their support and love during my study abroad.

There can never be enough words to thank my loving father in law Dr. Ghazi Nahar, who has showed me his support, care, encouragement. I want to thank my mother in law, my brothers and sister in law as well.

Last but not least, I would like to thank my colleagues, Ahmad Alhasanat, Nedal Alzoubi and Dr. Mohammad Ghazi, for their support and help. I also want to thank my dearest friends Khaldoon Radaideh, Khalid suwais, Ahmad Abu Shariha, Dr. Mohammad Bani Younes, Dr. Nihad Al\_Obaidi, Dr. Eid Abdel\_Munem, Adnan Hnaif, Qais Alhourani, Khalid Khazaeleh and Ahmad Abu Alrub for their care and support.

*Ahmad Saleem Alzoubi*

*Penang, Malaysia. February 2008.*

## TABLE OF CONTENTS

<b>Acknowledgements</b>	iii
<b>Table of Contents</b>	v
<b>List of Tables</b>	x
<b>List of Figures</b>	xii
<b>List of Abbreviations</b>	xxi
<b>List of Appendices</b>	xxii
<b>Abstrak</b>	xxiii
<b>Abstract</b>	xxv
<b>CHAPTER 1 – INTRODUCTION</b>	
1.1 Role of Breast Radiotherapy	1
1.2 Breast Anatomy	2
1.3 Treatment Field Arrangements	6
1.3.1 Breast and Chest Wall	6
1.3.2 Chest Wall and Lymph Nodes	8
1.3.3 Matching the Tangential Fields with the Supraclavicular Field	8
1.3.4 Matching the Tangential Fields with the Internal Mammary Field	9
1.4 Research Objectives	10
1.5 Structure of this Thesis	11
<b>CHAPTER 2 – LITERATURE REVIEW</b>	
2.1 Matchline of Supraclavicular and Tangential Breast Fields Techniques	13
2.2 Lung and Heart Dose during breast Radiotherapy	15

2.3	Entrance and Exit Dose for Breast Treatment	18
2.4	Contralateral Breast Dose during Breast Treatment	20
2.4.1	Contralateral Breast at Risk	20
2.4.2	Minimizing Contralateral Breast Dose	22

### **CHAPTER 3 – INSTRUMENTATION**

3.1	Introduction	24
3.2	Detectors	26
3.2.1	Thermoluminescent dosimeter	25
3.2.2	Si Diode	27
3.2.3	Film Dosimetry	28
3.2.4	Ion Chambers	29
3.3	TLD reader	31
3.3.1	Introduction	31
3.3.2	Heating System	31
3.3.3	Light Collection Unit	32
3.3.4	Nitrogen Gas Atmosphere	32
3.3.5	Glow Curve	34
3.4	Simulator	37
3.5	Linear Accelerator (LINAC)	38
3.6	Computed Tomography (Ct)	40
3.7	Phantoms	42
3.7.1	Solid Water Phantom	42
3.7.2	Heterogeneous Phantom	43

**CHAPTER 4 – DOSE DISTRIBUTION IN THE MATCH REGION OF  
SUPRACLAVICULAR AND TANGENTIAL BREAST  
FIELDS USING FOUR TECHNIQUES**

4.1	Introduction	46
4.2	Definition of Target Volume	47
4.3	Materials and Methods	51
4.3.1	Phantom	51
4.3.2	Dosimetry Equipment	54
4.3.3	Treatment Techniques	56
4.3.3.1	Technique A: Overlap Technique	56
4.3.3.2	Technique B: Couch Rotating Technique	56
4.3.3.3	Technique C: 5 mm Gap Asymmetric Jaw Technique	57
4.3.3.4	Technique D: 5mm Gap Symmetrical Field Technique	58
4.4	Results and Discussion	58
4.4.1	Response Behavior Of LiF:Mg;Ti TLD	58
4.4.1.1	Reproducibility	58
4.4.1.2	Linearity Response	61
4.4.1.3	Field Size Response	61
4.4.1.4	Angular Dependence	62
4.4.1.5	Effect of Wedge	64
4.4.1.6	Dose Rate Dependence	64
4.4.1.7	Percentage Depth Dose Curve (PDD)	66
4.4.2	Response Behavior of X-Omat V Film	67
4.4.2.1	Calibration Curve	67
4.4.2.2	Percentage Depth Dose Curve (PDD)	67

4.4.3 Treatment Techniques	69
4.4.3.1 Transversal Plane (Matchline Region Slice)	70
4.4.3.2 Sagittal Plane	72

**CHAPTER 5 – DETERMINATION OF ENTRANCE AND EXIT DOSES  
IN VIVO IN BREAST RADIOTHERAPY WITH A 6 MV  
PHOTON BEAM**

5.1 Introduction	93
5.2 Materials and Methods	94
5.2.1 Thermoluminescent LiF: Mg; Ti and LiF: Mg; Cu; P Dosimeters	94
5.2.2 VeriDose Diode n-type	97
5.2.2.1 Diode Calibration for Entrance and Exit Dose	100
5.2.3 Patient Dosimetry	102
5.3 Results and Discussion	104
5.3.1 TLD Calibration for Entrance and Exit Dose	104
5.3.2 Diode Calibration for Entrance and Exit Dose	106
5.3.3 Phantom Measurements	112
5.3.4 Patient Dosimetry	112

**CHAPTER 6 – CONTRALATERAL BREAST DOSE FROM CHEST  
WALL IRRADIATION – LOCAL EXPERIENCE**

6.1 Introduction	124
6.2 Material and Methods	125
6.2.1 TLD Calibration	125
6.2.2 Placement of TLDs in a Breast Phantom	126
6.2.3 Two Field & Three Field techniques	128

6.2.4	Patients	128
6.3	Results	129
6.3.1	TLD Calibration	129
6.3.2	Phantom Measurements	129
6.3.3	Patient Measurements	132
6.4	Discussion	142

## **CHAPTER 7 - CONCLUSION AND FUTURE WORKS**

7.1	Conclusion	145
7.2	Future Work	147
	References	148
	Appendices	160
	List of Publications	165

<b>LIST OF TABLES</b>		<b>Page</b>
Table 3.1	The half-life of the glow curve peaks of (TLD-100).	<b>34</b>
Table 3.2	Physical constants for the dosimeters and the materials used to simulate soft tissue and lung.	<b>44</b>
Table 4.1	Matchline transversal plane dose for overlap technique.	<b>79</b>
Table 4.2	Matchline transversal plane dose for couch rotating technique.	<b>79</b>
Table 4.3	Matchline transversal plane dose for 5 mm gap asymmetric jaw technique.	<b>79</b>
Table 4.4	Matchline transversal plane dose for 5 mm gap symmetrical field technique.	<b>79</b>
Table 4.5	Matchline sagittal plane maximum dose for overlap technique.	<b>92</b>
Table 4.6	Matchline sagittal plane maximum dose for couch rotating technique.	<b>92</b>
Table 4.7	Matchline sagittal plane maximum dose for 5 mm gap asymmetric jaw technique.	<b>92</b>
Table 4.8	Matchline sagittal plane maximum dose for 5 mm gap symmetrical field technique.	<b>92</b>
Table 5.1	Patient characteristics.	<b>104</b>
Table 5.2	Percent depth dose (PDD) (%) of skin of different measured methods and linacs from the literature. The methods include TLD extrapolation, black TLDs, Markus chamber (with Rawlinson correction), extrapolation chamber, parallel plate chamber, ultra-thin TLDs and LiF TLDs (This study).	<b>109</b>
Table 5.3	Calculated and measured (Diode and LiF 100H) entrance dose in phantom along matchline region using four different techniques.	<b>115</b>
Table 5.4	Calculated and measured (Diode and LiF100) entrance dose in phantom for tangential fields.	<b>115</b>
Table 5.5	Mean and median surface and $d_{\max}$ dose at matchline region.	<b>116</b>

Table 5.6	Mean and median surface and $d_{\max}$ dose to medial and lateral tangential fields.	<b>116</b>
Table 6.1	Patient characteristics.	<b>131</b>
Table 6.2	The contralateral breast mean dose ranges and the contribution of the prescribed dose reported by several authors using different treatment types include the present study.	<b>144</b>

<b>LIST OF FIGURES</b>		<b>Page</b>
Figure 1.1	Anatomy of the breast and lymphatic drainage. Anatomy of axilla (pectoralis major and minor muscles partially removed to demonstrate anatomic levels of lymph nodes).	<b>4</b>
Figure 1.2	Microscopic structure of the mammary gland. Ducts extend back from the nipple independent of one another, each defining a lobe of the breast. The major ducts arborize, culminating in the terminal lobular units. The ducts are lined by an epithelial layer in which ductal cancer is thought to arise. Most cancer is thought to arise in the extralobular terminal duct.	<b>5</b>
Figure 1.3	Anatomy of the lymphatic routes of the breast.	<b>5</b>
Figure 1.4	Anterior view of the patient set-up with medial tangential field. A Bright yellow: breast being treated, B Light yellow: beam in air, not touching woman, C Opening of the linear accelerator, D Arm holder supports woman's right arm.	<b>6</b>
Figure 1.5	Lateral view of the patient set-up with Lateral tangential field. A Bright yellow: breast being treated, B Light yellow: beam in air, not touching woman, C Opening of the linear accelerator, D Arm holder.	<b>7</b>
Figure 1.6	Cross-sectional view of patient receiving radiation to the breast area. A Middle radiation beam, B Side radiation beam, C Bright yellow: place where radiation is given to the breast, D Rib cage/chest wall, E Heart, F Lungs, G Backbone, H Sternum / breastbone.	<b>7</b>
Figure 1.7	Anterior view for three-field technique.	<b>8</b>
Figure 1.8	Diagrams showing several relationships between internal mammary and tangential fields. (A) A significant cold region exists if the internal mammary (IM) tangential matchline overlies a large amount of breast tissue. (B) The cold area may be negligible if the breast tissue beneath the matchline is thin. (C) The lack of a separate IM field can result in irradiation of an excessive volume of lung, particularly in large-chested patients.	<b>10</b>
Figure 3.1	Nuclear Associates, VeriDose diodes.	<b>27</b>
Figure 3.2	Wellhofer farmer type ionization chamber FC65-G.	<b>30</b>

Figure 3.3	The Harshaw TLD reader model 3500 which was used in the experiment.	<b>32</b>
Figure 3.4	Schematic diagrams showing the features of a TLD reader.	<b>32</b>
Figure 3.5	Schematic diagrams showing the principle of TLD reader heating system with temperature feedback.	<b>33</b>
Figure 3.6	Typical arrangement of the light collection unit of a TLD reader.	<b>33</b>
Figure 3.7	Glow curves for LiF: Mg, Ti (TLD 100) annealed for 1 hr at 400°C followed by: A, cooling ( $10^3$ °C / min) to normal ambient temperature; B, 16 hr anneal at 80°C, followed by irradiation.	<b>35</b>
Figure 3.8	Glow curves for LiF: Mg;Cu;P (TLD 100H).	<b>35</b>
Figure 3.9	Glow curves for LiF: Mg, Ti (TLD 100).	<b>36</b>
Figure 3.10	Two types of simulators. A: Simview NT Simulator, B: Varian-TEM Ximatron Simulator.	<b>37</b>
Figure 3.11	Block diagram of typical medical linear accelerator.	<b>39</b>
Figure 3.12	Components of the Treatment Head. A: X-ray therapy mode. B: Electron therapy mode.	<b>39</b>
Figure 3.13	SOMATOM Sensation Open CT Scanners for Virtual Simulation.	<b>41</b>
Figure 3.14	Water solid phantoms, A: Plastic water equivalent phantom, Nuclear Associates and B: Gammex RMI solid water phantom.	<b>42</b>
Figure 3.15	Heterogeneous phantom.	<b>45</b>
Figure 4.1	Schematic representation of "volumes" in radiation therapy. (Taken from ICRU. Prescribing, recording, and reporting photon beam therapy.	<b>50</b>
Figure 4.2	Heterogeneous breast phantom.	<b>53</b>
Figure 4.3	Four techniques of three field treatment beam geometry in irradiation of the breast and supraclavicular fields studied in this investigation. Techniques illustrated in anterior, lateral, and transversal views.	<b>60</b>

Figure 4.4	Linearity of thermoluminescence (TLD) against absorbed dose.	<b>61</b>
Figure 4.5	Output factor for TLD and ion chamber.	<b>62</b>
Figure 4.6	Angular dependence of TLDs.	<b>63</b>
Figure 4.7	Angular dependence of TLDs.	<b>65</b>
Figure 4.8	Wedge correction factor for TLD.	<b>65</b>
Figure 4.9	SSD dependence of TLD.	<b>66</b>
Figure 4.10	Dose rate for TLD using various SSD.	<b>66</b>
Figure 4.11	PDD curve in 'solid water' phantom (Gamex RMI, USA) and Pespex phantom for a 10 x 10 cm <sup>2</sup> field at an SSD of 100 cm for 6 MV photon beam using LiF 100 TLDs and ion chamber.	<b>68</b>
Figure 4.12	Sensitometric response of Kodak X-Omat V film for 6 MV photon beams.	<b>68</b>
Figure 4.13	PDD curve in 'solid water' phantom (Gamex RMI, USA) for a 10 x 10 cm <sup>2</sup> field at an SSD of 100 cm for 6 MV photon beam using Kodak X-Omat V film.	<b>69</b>
Figure 4.14	Isodose distributions for transversal plane on the matchline planning slice generated by pencil beam dose algorithms for overlap technique. Axial CT slice through the phantom with positions of TL dosimeters (Black circles) in the heterogeneous phantom. Field borders, CTV, and lungs are depicted.	<b>75</b>
Figure 4.15	Comparison between calculation and measurements dose along the matchline of the tangential and supraclavicular fields for overlap technique. The dose distribution in transversal plane for different depths, 1.5 cm, 2.5 cm, 4.5 cm, and 6.5 cm from the anterior surface measured at the level of the matchline.	<b>75</b>
Figure 4.16	Isodose distributions for transversal plane on the matchline planning slice generated by pencil beam dose algorithms for couch rotating technique. Axial CT slice through the phantom with positions of TL dosimeters (Black circles) in the heterogeneous phantom. Field borders, CTV, and lungs are depicted.	<b>76</b>

Figure 4.17	Comparison between calculation and measurements dose along the matchline of the tangential and supraclavicular fields for couch rotating technique. The dose distribution in transversal plane for different depths, 1.5 cm, 2.5 cm, 4.5 cm, and 6.5 cm from the anterior surface measured at the level of the matchline.	<b>76</b>
Figure 4.18	Isodose distributions for transversal plane on the matchline planning slice generated by pencil beam dose algorithms for 5 mm gap asymmetric jaw technique. Axial CT slice through the phantom with positions of TL dosimeters (Black circles) in the heterogeneous phantom. Field borders, CTV, and lungs are depicted.	<b>77</b>
Figure 4.19	Comparison between calculation and measurements dose along the matchline of the tangential and supraclavicular fields for 5 mm gap asymmetric jaw technique. The dose distribution in transversal plane for different depths, 1.5 cm, 2.5 cm, 4.5 cm, and 6.5 cm from the anterior surface measured at the level of the matchline.	<b>77</b>
Figure 4.20	Isodose distributions for transversal plane on the matchline planning slice generated by pencil beam dose algorithms for 5 mm gap symmetrical field technique. Axial CT slice through the phantom with positions of TL dosimeters (Black circles) in the heterogeneous phantom. Field borders, CTV, and lungs are depicted.	<b>78</b>
Figure 4.21	Comparison between calculation and measurements dose along the matchline of the tangential and supraclavicular fields for 5 mm gap symmetrical field technique. The dose distribution in transversal plane for different depths, 1.5 cm, 2.5 cm, 4.5 cm, and 6.5 cm from the anterior surface measured at the level of the matchline.	<b>78</b>
Figure 4.22	Isodose distributions for sagittal plane (a, b, c) for the matchline planning slices generated by pencil beam dose algorithms for overlap technique. Sagittal plane CT slices through the phantom with positions of Field borders, CTV, and lungs are depicted in the heterogeneous phantom.	<b>80</b>
Figure 4.23	Comparison between calculation and measurements dose along the matchline of the tangential and supraclavicular fields for overlap technique. The dose distribution in sagittal plane at 1.5 cm depth for various locations, (a) 4 cm, (b) 7 cm, and (c) 11 cm lateral to the midline.	<b>81</b>

Figure 4.24	Comparison between calculation and measurements dose along the matchline of the tangential and supraclavicular fields for overlap technique. The dose distribution in sagittal plane at 4.5 cm depth for various locations, (a) 4 cm, (b) 7 cm, and (c) 11 cm lateral to the midline.	<b>82</b>
Figure 4.25	Isodose distributions for sagittal plane (a, b, c) for the matchline planning slices generated by pencil beam dose algorithms for couch rotating technique. Sagittal plane CT slices through the phantom with positions of Field borders, CTV, and lungs are depicted in the heterogeneous phantom.	<b>83</b>
Figure 4.26	Comparison between calculation and measurements dose along the matchline of the tangential and supraclavicular fields for couch rotating technique. The dose distribution in sagittal plane at 1.5 cm depth for various locations, (a) 4 cm, (b) 7 cm, and (c) 11 cm lateral to the midline.	<b>84</b>
Figure 4.27	Comparison between calculation and measurements dose along the matchline of the tangential and supraclavicular fields for couch rotating technique. The dose distribution in sagittal plane at 4.5 cm depth for various locations, (a) 4 cm, (b) 7 cm, and (c) 11 cm lateral to the midline.	<b>85</b>
Figure 4.28	Isodose distributions for sagittal plane (a, b, c) for the matchline planning slices generated by pencil beam dose algorithms for 5 mm gap asymmetric jaw technique. Sagittal plane CT slices through the phantom with positions of Field borders, CTV, and lungs are depicted in the heterogeneous phantom.	<b>86</b>
Figure 4.29	Comparison between calculation and measurements dose along the matchline of the tangential and supraclavicular fields for 5 mm gap asymmetric jaw technique. The dose distribution in sagittal plane at 1.5 cm depth for various locations, (a) 4 cm, (b) 7 cm, and (c) 11 cm lateral to the midline.	<b>87</b>
Figure 4.30	Comparison between calculation and measurements dose along the matchline of the tangential and supraclavicular fields for 5 mm gap asymmetric jaw technique. The dose distribution in sagittal plane at 4.5 cm depth for various locations, (a) 4 cm, (b) 7 cm, and (c) 11 cm lateral to the midline.	<b>88</b>

Figure 4.31	Isodose distributions for sagittal plane (a, b, c) for the matchline planning slices generated by pencil beam dose algorithms for 5 mm gap symmetrical field technique. Sagittal plane CT slices through the phantom with positions of Field borders, CTV, and lungs are depicted in the heterogeneous phantom.	<b>89</b>
Figure 4.32	Comparison between calculation and measurements dose along the matchline of the tangential and supraclavicular fields for 5 mm gap symmetrical field technique. The dose distribution in sagittal plane at 1.5 cm depth for various locations, (a) 4 cm, (b) 7 cm, and (c) 11 cm lateral to the midline.	<b>90</b>
Figure 4.33	Comparison between calculation and measurements dose along the matchline of the tangential and supraclavicular fields for 5 mm gap symmetrical field technique. The dose distribution in sagittal plane at 4.5 cm depth for various locations, (a) 4 cm, (b) 7 cm, and (c) 11 cm lateral to the midline.	<b>91</b>
Figure 5.1	(A) The PDD measurement setup. (B) Cylindrical phantom measurement setup: perspex cylindrical phantom.	<b>98</b>
Figure 5.2	Oblique factor measurement setup.	<b>98</b>
Figure 5.3	Anterior view of the fabricated heterogeneous phantom with TLD positions. B: at the central axis of SCF, A: 3 cm lateral from B, C: 3 cm medial from B, D: at CAX of tangential fields in the lateral-medial direction and E: at CAX of tangential fields in the medial-lateral direction.	<b>99</b>
Figure 5.4	Determination of the entrance and exit dose calibration factors of a detector (diode or TL dosimeter). The calibrated ionization chamber is put at $d_{\max}$ depth for the entrance dose calibration factor (A) or at a distance $d_{\max}$ from the exit side of the field for the exit dose calibration (B) and the detector is positioned at the entrance or exit surface, respectively.	<b>103</b>
Figure 5.5	TLD 100 entrance calibration linear fit.	<b>108</b>
Figure 5.6	TLD 100H entrance calibration linear fit.	<b>108</b>
Figure 5.7	Percent depth dose of 6 MV photons with various field sizes.	<b>110</b>
Figure 5.8	Dose ratios (oblique factor) of 6 MV photons with various incident angles of beam.	<b>110</b>

Figure 5.9	The surface dose of 6MV photon at various positions on the cylindrical phantom to dose 100 cGy at the center of phantom.	<b>110</b>
Figure 5.10	Entrance dose calibration of diode at 6 MV photon beam.	<b>111</b>
Figure 5.11	Exit dose calibration line of diode under full backscatter condition.	<b>111</b>
Figure 5.12	Ratio of measured to expected dose at surface (match region)in 66 measurements from 22 patients using LiF 100H TLD.	<b>117</b>
Figure 5.13	The calculated surface dose (using the pencil beam algorithm) plotted against the measured surface dose using LiF 100H TLD at match region. Individual data for 22 patients are presented.	<b>117</b>
Figure 5.14	Ratio of measured to expected dose at surface in 66 measurements from 22 patients using LiF 100 TLD.	<b>118</b>
Figure 5.15	The calculated surface dose (using the pencil beam algorithm) plotted against the measured surface dose using LiF 100 TLD for tangential fields. Individual data for 22 patients are presented.	<b>118</b>
Figure 5.16	Ratio of measured to expected dose at $D_{max}$ (match region) in 66 measurements from 22 patients using LiF 100H TLD.	<b>119</b>
Figure 5.17	The calculated $D_{max}$ dose (using the pencil beam algorithm) plotted against the measured $D_{max}$ dose using LiF 100H TLD at match region. Individual data for 22 patients are presented.	<b>119</b>
Figure 5.18	Histogram and Gaussian plot of patient entrance dose measurements: TLD's overall results.	<b>120</b>
Figure 5.19	Ratio of measured to expected dose at $D_{max}$ in 66 measurements from 22 patients using LiF 100 TLD.	<b>120</b>
Figure 5.20	The calculated $D_{max}$ dose (using the pencil beam algorithm) plotted against the measured $D_{max}$ dose using LiF 100 TLD for tangential fields. Individual data for 22 patients are presented.	<b>121</b>
Figure 5.21	Ratio of measured to expected dose at $D_{max}$ (match region) in 66 measurements from 22 patients.	<b>121</b>
Figure 5.22	The calculated $D_{max}$ (using the pencil beam algorithm) plotted against the measured $D_{max}$ . Individual data for 22 patients are presented.	<b>122</b>

Figure 5.23	Ratio of measured to expected dose at $D_{\max}$ in 68 measurements from 34 patients.	<b>122</b>
Figure 5.24	The calculated $D_{\max}$ (using the pencil beam algorithm) plotted against the measured $D_{\max}$ . Individual data for 34 patients are presented.	<b>123</b>
Figure 6.1	Anterior view of the fabricated heterogeneous phantom.	<b>130</b>
Figure 6.2	Axial CT slice through the phantom with positions of TL dosimeters (Black circles) in the heterogeneous phantom. Field borders, CTV, lungs, heart, and spinal cord are also depicted.	<b>130</b>
Figure 6.3	Calibration of TLDs at the surface and at $d_{\max}$ of the solid water phantom.	<b>133</b>
Figure 6.4(a)	Mean measured dose and calculated dose for trace A which is at the level of central axis of tangential field in the medial-lateral direction.	<b>133</b>
Figure 6.4(b)	Mean measured dose and calculated dose for trace B which is 3 cm inferior to trace A.	<b>134</b>
Figure 6.4(c)	Mean measured dose and calculated dose for trace C which is 6 cm inferior to trace A	<b>134</b>
Figure 6.5	Ratio of mean measured to expected dose at Surface in 24 measurements.	<b>135</b>
Figure 6.6	Ratio of mean measured to expected dose at $d_{\max}$ in 24 measurements.	<b>135</b>
Figure 6.7	Measured and calculated internal doses at the 3 different slices and at the 3 depths in the current 3-field treatment technique. The points are located internally in CB of the phantom.	<b>136</b>
Figure 6.8(a)	Mean measured dose and calculated dose at trace A (At central axis of tangential field, medial-lateral direction) for the 3 groups of patients. G1: Mastectomy tangential fields (2 field treatment), G2 : Mastectomy 3 field treatment, G3: Full breast 3 field treatment.	<b>136</b>
Figure 6.8(b)	Mean measured and calculated dose for trace B (3 cm inferior to the central axis of tangential field, medial-lateral direction) G1: Mastectomy tangential fields (2 field treatment), G2 : Mastectomy 3 field treatment, G3: Full breast 3 field treatment.	<b>137</b>

Figure 6.8(c)	Mean measured and calculated dose for trace C (6 cm inferior to the central axis of tangential field, medial-lateral direction).	<b>137</b>
Figure 6.9(a)	Ratio of mean measured to expected dose at Surface for Trace A.	<b>138</b>
Figure 6.9(b)	Ratio of mean measured to expected dose at $d_{max}$ for Trace A.	<b>138</b>
Figure 6.10(a)	Ratio of mean measured to expected dose at Surface for Trace B.	<b>139</b>
Figure 6.10(b)	Ratio of mean measured to expected dose at $d_{max}$ for Trace B.	<b>139</b>
Figure 6.11(a)	Ratio of mean measured to expected dose at Surface for Trace C.	<b>140</b>
Figure 6.11(b)	Ratio of mean measured to expected dose at $d_{max}$ for Trace C.	<b>140</b>
Figure 6.12	Patient dose distribution at $d_{max}$ at 2 cm and 12 cm in the medial lateral direction for the three traces.	<b>141</b>
Figure 6.13	Ratio of mean TLD measured to expected dose for nipple position at $d_{max}$ in 100 measurements for 25 patients.	<b>141</b>

## LIST OF ABBREVIATIONS

CB	Contralateral Breast
TLD	Thermoluminescent Dosimeter
TL	Thermoluminescent
TPS	Treatment Planning System
3D-CRT	Three-Dimensional Conformal Radiation Therapy
DCIS	Ductal Carcinoma in Situ
ASTRO	American Society for Therapeutic Radiology and Oncology
PMRT	Post-Mastectomy Radiation Therapy
CT	Computed Tomography
IM	Internal Mammary
LINAC	Linear Accelerator
PMT	Photomultiplier Tube
MU	Monitoring Unit
LiF	Lithium Fluoride
ESTRO	European Society for Therapeutic Radiology and Oncology
$D_{\max}$	Maximum Dose
SAD	Source-to-Axis Distance
SSD	Source-to-Skin Distance
LET	Linear Energy Transfer
SCF	Supraclavicular Field
ICRU	International Commission on Radiation Units and Measurements
GTV	Gross Tumor Volume
CTV	Clinical Target Volume
PTV	Planning Target Volume
OAR	Organs at Risk
DVH	Dose Volume Histogram
ECC	Elemental Correction Coefficients
CF	Correction Factor

## **LIST OF APPENDICES**

Appendix A	Parameters Affect Diode Measurements	<b>160</b>
Appendix B	Patients Calculation Sheet	<b>164</b>
Appendix C	TLD-100 reproducibility	<b>169</b>

# **RADIOTERAPI SELEPAS MASTEKTOMI YANG MELIBATKAN NOD SUPRAKLAVIKAL - DOS GARIS TINDIHAN, DOS TUMOR DAN DOS ORGAN BERISIKO**

## **ABSTRAK**

Tujuan kajian ini ialah untuk menyelidiki kesan pertindihan akibat daripada pencapahan alur medan tangen terhadap medan supraklavikal dalam penyinaran payu dara pesakit yang menerima rawatan radioterapi payu dara, meneliti dos terserap dalam kulit pesakit untuk rawatan tersebut dan menentukan dos dalam payu dara kontralateral (CB) dalam fantom yang difabrikasi dan juga dalam pesakit bagi teknik 2-medan dan teknik 3-medan yang digunakan dalam penyinaran dinding dada selepas mastektomi.

Fantom heterogen torso wanita dewasa bersaiz sederhana yang difabrikasi, satu set dosmeter termoluminesen (TLD), filem terapi megavoltan, dan diod VeriDose jenis-n telah digunakan untuk pengukuran dos. Empat teknik yang berbeza telah digunakan dalam kajian ini; teknik pertindihan, teknik katil berputar yang digunakan secara rutin di Pusat Kanser Mount Miriam, Pulau Pinang, teknik jurang 5 mm menggunakan rahang tak simetri untuk menghalang medan supraklavikal yang digunakan secara rutin di Hospital Pantai Mutiara, Pulau Pinang dan teknik jurang 5 mm menggunakan medan bersimetri. Semua rawatan telah dilaksanakan menggunakan terapi sinaran 3-dimensi berbentuk menggunakan alur foton 6 MV. Sistem perancang rawatan (TPS) (Plato RPS V2.6.3, Nucletron) menggunakan algoritma alur pensel untuk penghitungan dos. Penghitungan dos TPS telah dinormalkan terhadap isopusat medan tangen dan terhadap  $d_{maks}$  untuk medan supraklavikal.

Tiga satah sagital daripada medan supraklavikal hingga ke medan tangen dan satu satah melintang sepanjang garis sepadan bagi ketiga-tiga medan dipilih untuk membandingkan dos yang dihitung dan yang diukur dalam rantau sepadan. Pengukuran dos dilaksanakan terhadap 34 pesakit yang menerima rawatan radioterapi alur luar di Pusat Kanser Mount Miriam dalam tempoh masa antara Jun 2008 dan September 2008.

Min penghasilan semula bacaan TLD dan filem berkisar pada 3 % bagi satu sisihan piawai. Dos daripada filem dan TLD telah dibandingkan dengan dos yang dihitung daripada TPS. Dos yang diukur dan dihitung di rantau sepadan yang dipilih adalah sama di sekitar 11 % untuk filem dan di sekitar 12 % untuk TLD. Apabila kesepadanan, jurang dan pertindihan dicapai untuk pengukuran yang teliti dalam fantom, ketakpastian total untuk diod bagi kedua-dua penentukuran dos masuk dan dos keluar adalah dalam lingkungan 5 % untuk keadaan rujukan dan bukan rujukan. Secara penghampirannya dos keluar dan dos masuk yang diukur dan dihitung untuk pesakit mempunyai perhubungan linear di antara satu sama lain untuk. Nisbah purata dos CB yang diukur terhadap dos CB yang dihitung menggunakan algoritma alur pensel adalah lebih kurang 53 % sementara pada  $d_{maks}$ , nisbahnya adalah  $< 11 \%$ . Min dan median dos CB dalaman yang diukur pada kedalaman berbeza dalam fantom pada permukaan adalah  $5.47 \pm 0.22$  cGy dan 5.44 cGy masing-masing.

# **POST-MASTECTOMY RADIOTHERAPY INVOLVING SUPRACLAVICAL NODES – MATCHLINE DOSE, TUMOUR DOSE AND ORGANS AT RISK DOSE**

## **ABSTRACT**

The purposes of this study were investigated the effect of the overlap resulting from the beam divergence of the tangential fields onto a supraclavicular field in breast irradiation of patients undergoing breast radiotherapy, to examine the absorbed dose to the skin of patients in such treatments and to determine the dose in contralateral breast (CB) from 2-field and 3-field techniques used in post-mastectomy chest wall irradiations in a fabricated phantom as well as in patients.

A heterogeneous fabricated phantom of an adult medium female torso, a set of thermoluminescent dosimeters (TLDs), megavoltage therapy films, and an n-type VeriDose diode were used in the dose measurements. Four different techniques were used in this study, overlap technique, couch rotating technique which is routinely applied in Mount Miriam Cancer Centre, Penang, a gap of 5 mm technique using asymmetric jaws to block the supraclavicular field which is routinely applied in Pantai Mutiara Hospital, Penang, and a 5 mm gap technique using symmetrical field. All treatments have been done with three-dimensional conformal radiation therapy (3D-CRT) using 6 MV photon beams. The treatment planning system (TPS) (Plato RPS V2.6.3, Nucletron) uses the pencil beam algorithm for dose calculations. The TPS dose calculations were normalized at the isocentre of the tangential fields and at  $d_{\max}$  for the supraclavicular field.

Three sagittal planes from the supraclavicular field down to the tangential fields and one transversal plane along the match line of the three fields were selected to compare the measured and calculated dose in the match region. Dose

measurements were performed on thirty-four patients undergoing external beam radiotherapy at the Mount Miriam Cancer Centre, during the period between June 2008 and September 2008

The mean reproducibility of TLD and film readings was within 3% for one standard deviation. Doses from films and TLDs were compared to the calculated doses from the TPS. In the matching selected regions, the measured and calculated doses agreed within 11 % for films and 12 % for TLDs. In phantom, where care was taken to achieve the necessary match, gap and overlap, the total uncertainty for the diode from both the entrance and the exit dose calibration was within 5 % for reference and non-reference conditions. The measurements and calculations doses for the patients are approximately linearly related to each other for entrance and exit dose. The average ratio of the measured to the calculated CB dose using the pencil beam algorithm was approximately 53% while at  $d_{\max}$  the ratio was < 11%. The mean and median measured internal CB dose at different depths in a phantom at surface was  $5.47 \pm 0.22$  cGy and 5.44 cGy respectively.

## CHAPTER 1

### INTRODUCTION

#### 1.1 Role of Breast Radiotherapy

Radiotherapy is given for primary carcinoma of the breast to reduce recurrence. Researchers have found that radiotherapy is beneficial for patients particularly for improving survival after mastectomy. The removal of lymph glands containing cancer cells results in the need for radiotherapy for the remaining areas to reduce the risk of recurrence. For example, after mastectomy, radiotherapy may be given to the chest wall if the tumour is more than 5 cm in diameter (Dobbles *et al.*, 1999).

Often radiotherapy may be used before, or instead of, surgery. For inoperable T<sub>3</sub> and T<sub>4</sub> tumours, various strategies are involved such as the inclusion of chemotherapy or hormone therapy. Operable tumours 3 – 4 cm or more in diameter is candidate for recurrence if radiotherapy is used in conjunction with conservative surgery, and therefore chemotherapy is more preferred (Dobbles *et al.*, 1999).

In Malaysia breast cancer is the dominant type of female cancer and is affecting one in 19 women and over 4000 new cases is reported annually (<http://www.makna.org.my/breastcancer.asp>, 2008). In the United States the projected breast cancer incidence was 178,480 in 2007 (Jemal *et al.*, 2007). Total mastectomy is normally performed for approximately 60-70 % of the reported cases in Malaysia followed by radiotherapy. According to the American Society for Therapeutic Radiology and Oncology (ASTRO) guidelines, post-mastectomy radiation therapy (PMRT) is recommended for patients with tumours > 5 cm and / or

with > 4 positive axillary lymph nodes. PMRT is also considered when patients have negative nodes but have adverse multiple features such as primary tumour > 2 cm, unsatisfactory surgical margins and lymphovascular invasion (Bese *et al.*, 2006).

The increase in survival manifests in a study of mastectomy. On the lighter side, more positive cosmetic appearance of the breasts of some patients after radiotherapy was observed. This highlights the role of radiotherapy. For conservative surgery, some study indicates that it actually decreases the incidence of Ductal Carcinoma in Situ (DCIS) recurrence and development of invasive diseases.

The presence of high grade malignancy tumour if incompletely excised or if there is tumour close to the excision margin constitutes a high risk factor and calls for the application of radiotherapy to the chest wall. In other cases however, irradiation is unnecessary such as when an axillary dissection up to the lower border of the pectoralis minor is not done. However if axillary nodes are involved, radiation may be given to the axilla and supraclavicular fossa.

Tumours in the central and medial quadrant require irradiation to the internal mammary nodes. Past experiences have shown that local recurrences are rare in these circumstances and therefore routine radiotherapy is not recommended. Other related method of control for recurrence such as in the case of critical breast conservation is the adoption of interstitial implantation. This will give a boost to the site of excision following lumpectomy and external beam radiation as part of the treatment.

## **1.2 Breast Anatomy**

The breast is made up of the mammary gland, fat, blood vessels, nerves, and lymphatics as shown in Fig. 1.1. (Kopans, 1987; Haagensen, 1971) The surface of the breast has deep attachments of fibrous septa, called Cooper's ligament, which runs between the superficial fascia (attached to the skin) and the deep fascia

(covering the pectoralis major and other muscles of the chest wall). (Del Regato *et al.*, 1977).

The mammary gland lies over the pectoralis major muscle and extends from the second to the sixth rib in the vertical plane and from the sternum to the anterior or even midaxillary line. (Del Regato *et al.*, 1977) An additional layer of mammary tissue extends laterally into the axilla to a variable degree. This axillary projection, often called the tail, is sometimes quite prominent and should always be kept in mind during examinations and in planning radiation therapy.

The retro mammary bursa lies between the deep layer of the superficial fascia and the deep fascia; it contains loose areolar tissue that allows for mobility over the chest wall. (Haagensen, 1971) It is crossed by projections of the deep layer of the superficial fascia that joins with the deep pectoral fascia to form the posterior suspensory ligaments of the breast. Deep projections of mammary parenchyma may extend between the muscle bundles of the pectoralis major muscle. The mammary consists of glandular tissue arranged in multiple lobes composed of lobules connected in ducts, areolar tissue, and blood vessels. The smallest lobules consist of clusters of rounded alveoli that open into the small branches of the lactiferous ducts (Fig. 1.2); these unite and form larger ducts that eventually converge into single canals in the nipple, corresponding to each lobe of the gland (15 to 20 galactophori). (Kopans, 1989).

A network of lymphatics is formed over the entire surface of the chest, neck, and abdomen and becomes dense under the areola. Mammary gland lymphatics begin in the interlobular or prelobular spaces, follow the ducts, and end in the subareolar network of lymphatics of the skin. (Del Regato *et al.*, 1977; Haagensen, 1971) The following lymphatic pathways originate mostly in the base of the breast:

(1) the axillary or principal pathway passes from the upper and lower halves of the breast to the lateral chain of nodes situated between the second and third intercostal space; (2) the transpectoral pathway passes through the pectoralis major muscle to the supraclavicular lymph nodes; and (3) the internal mammary pathway passes through the midline, through the pectoralis major and intercostal muscles, usually close to the sternum, to the nodes of the internal mammary chain. The main lymphatic channels of the breast are illustrated in Fig. 1.3.

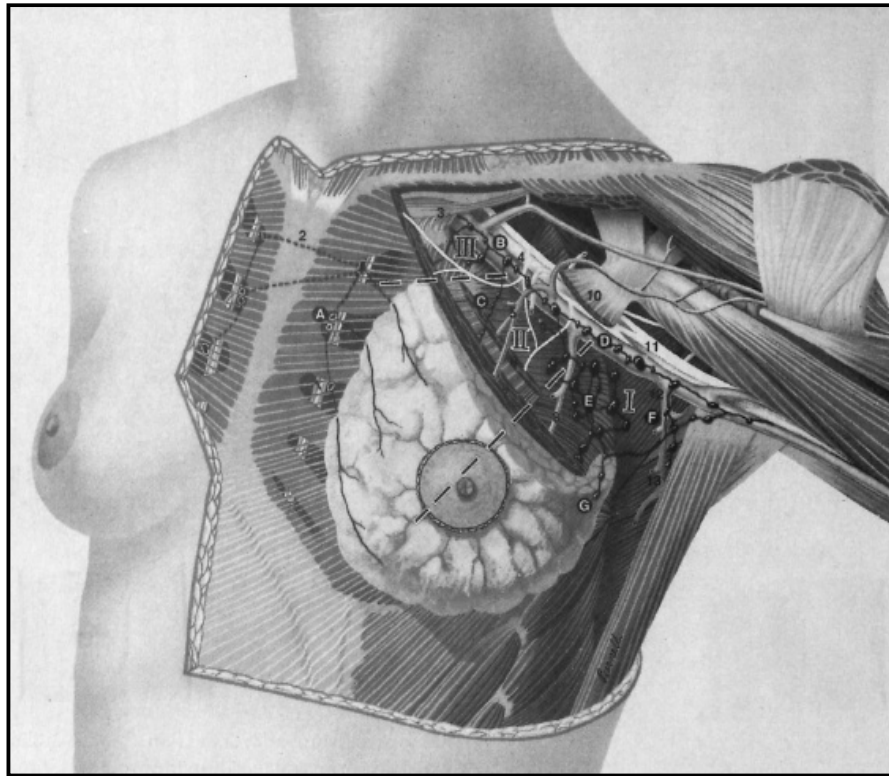


Figure 1.1: Anatomy of the breast and lymphatic drainage. Anatomy of axilla (pectoralis major and minor muscles partially removed to demonstrate anatomic levels of lymph nodes). Internal mammary artery and vein (1), substernal cross drainage to contralateral internal mammary lymphatic chain (2); subclavian muscle and Halsted's ligament (3); lateral pectoral nerve (from lateral cord) (4); pectoral branch from thoracoacromial vein (5); pectoralis minor muscle (6); pectoralis major muscle (7); lateral thoracic vein (8); medial pectoral nerve (from medial cord) (9); pectoralis minor muscle (10); median nerve (11); subcapsular vein (12); thoracodorsal vein (13); internal mammary lymph nodes (A); apical lymph nodes (B); interpectoral (Rotter's) lymph nodes (C); axillary vein lymph nodes (D); central lymph nodes (E); scapular lymph nodes (F); external mammary lymph nodes (G). Level I lymph nodes lateral to lateral border of pectoralis minor muscle; level II lymph nodes

behind pectoralis minor muscle; level III lymph nodes medial to medial border of pectoralis minor muscle. (Osborne, 1987)

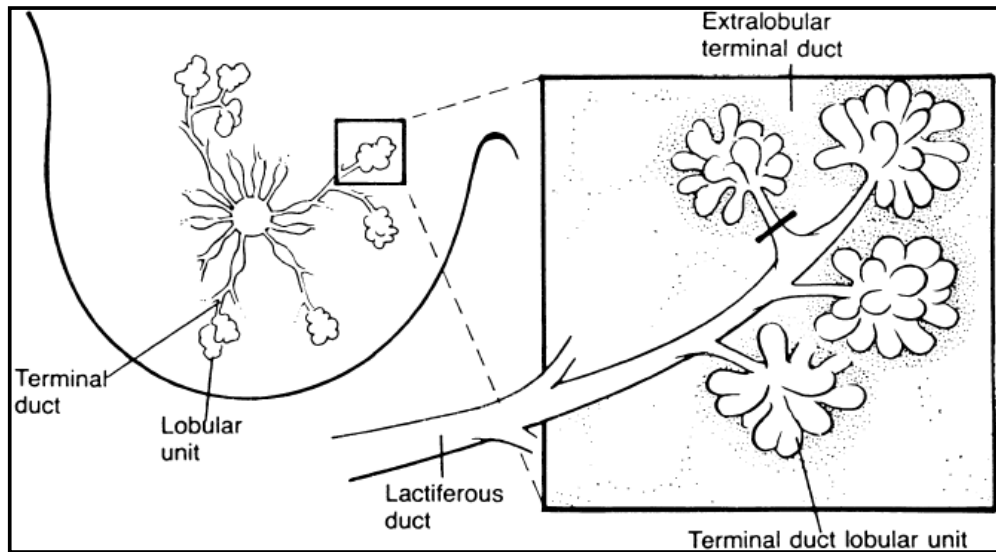


Figure 1.2: Microscopic structure of the mammary gland. Ducts extend back from the nipple independent of one another, each defining a lobe of the breast. The major ducts arborize, culminating in the terminal lobular units. The ducts are lined by an epithelial layer in which ductal cancer is thought to arise. Most cancer is thought to arise in the extralobular terminal duct. (Kopans, 1989)

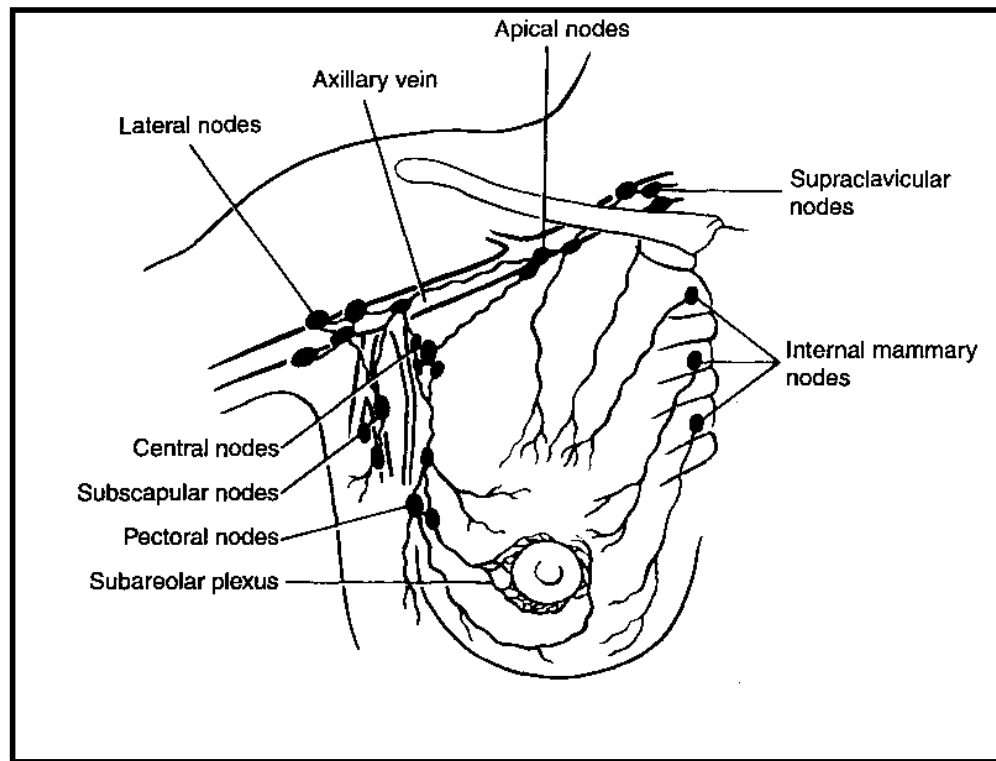


Figure 1.3: Anatomy of the lymphatic routes of the breast. (Dobbes *et al.*, 1999).

### 1.3 Treatment Field Arrangements

The patient lies supine on the simulator couch with a suitable immobilization, the position of the patient aligned using laser lights. The field's borders are marked on the skin with the centre points of medial and lateral fields. Three reference tattoo points are made at medial, lateral field centres, and at the opposite side of the body.

#### 1.3.1 Breast and Chest Wall

The most common set-up for breast cancer patients is a two field x-ray approach with the patient supine, ipsilateral arm above head (Murshed, 2006) as shown in Fig. 1.4. The first field is the medial tangent field and the second is the lateral tangent field. The medial tangent field border starts at the patient midline, it involves the linac gantry to be positioned over the patient and slightly off to one side so the beam can enter the breast at a tangential angle. Figure 1.5 shows the lateral field with gantry positioned off to the ipsilateral side and slightly below the table level. Figure 1.6 shows transversal plane of the fields for two beam open field therapy.

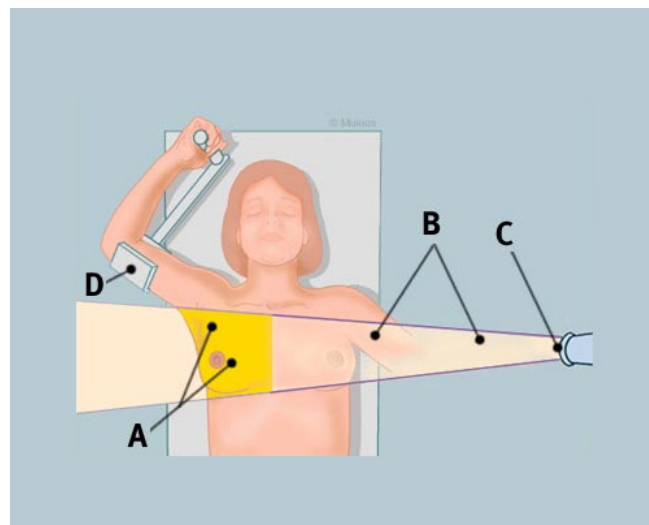


Figure 1.4: Anterior view of the patient set-up with medial tangential field. **A** Bright yellow: breast being treated, **B** Light yellow: beam in air, not touching woman, **C** Opening of the linear accelerator, **D** Arm holder supports woman's right arm (Taken from <http://www.breastcancer.org/treatment/radiation/types/ext/>)

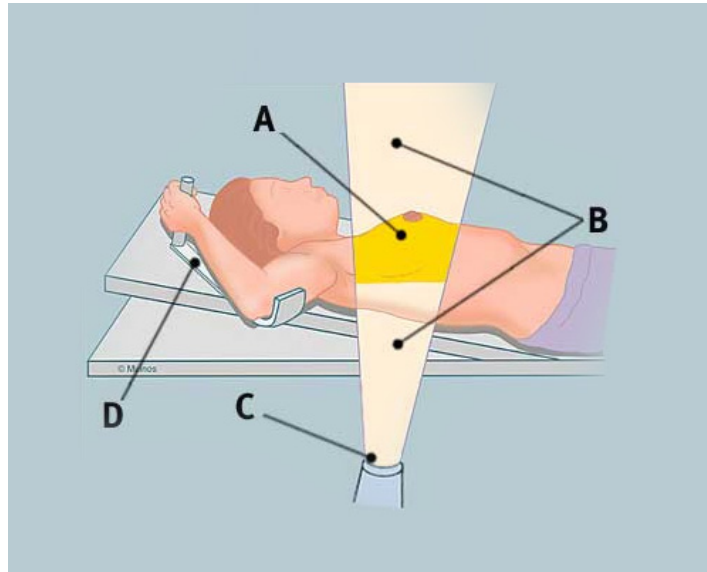


Figure 1.5: Lateral view of the patient set-up with Lateral tangential field. **A** Bright yellow: breast being treated, **B** Light yellow: beam in air, not touching woman, **C** Opening of the linear accelerator, **D** Arm holder (Taken from <http://www.breastcancer.org/treatment/radiation/types/ext/>)

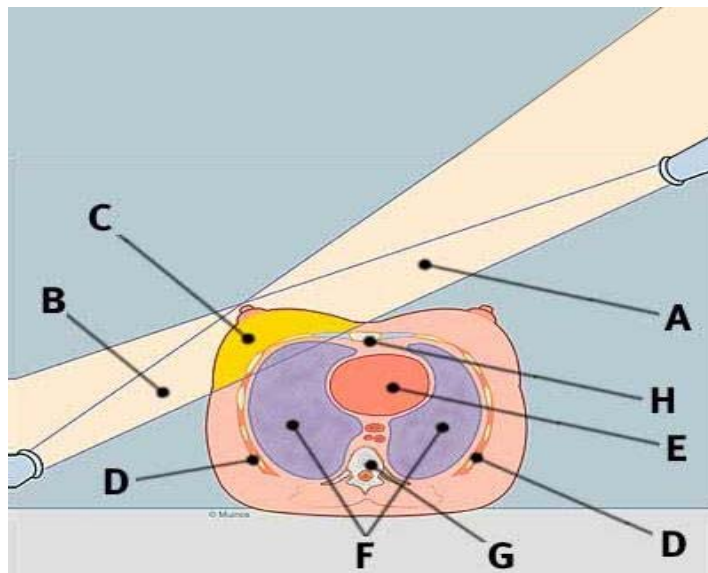


Figure 1.6: Cross-sectional view of patient receiving radiation to the breast area. **A** Middle radiation beam, **B** Side radiation beam, **C** Bright yellow: place where radiation is given to the breast, **D** Rib cage/chest wall, **E** Heart, **F** Lungs, **G** Backbone, **H** Sternum / breastbone. (Taken from <http://www.breastcancer.org/treatment/radiation/types/ext/>)

### 1.3.2 Chest Wall and Lymph Nodes

The two tangential fields are used for treating the breast or chest wall. A single anterior field can be used to irradiate the supraclavicular nodes only as shown in Fig. 1.7. The superior border extends at least 3 cm above the medial end of the clavicle. Medial border is placed 1 cm apart to the patient midline to avoid the larynx and spinal cord. Lateral border lies at the junction of the medial two-thirds and the lateral one-third of the clavicle. The inferior border is at the lower border of the clavicle (Dobbles *et al.*, 1999).

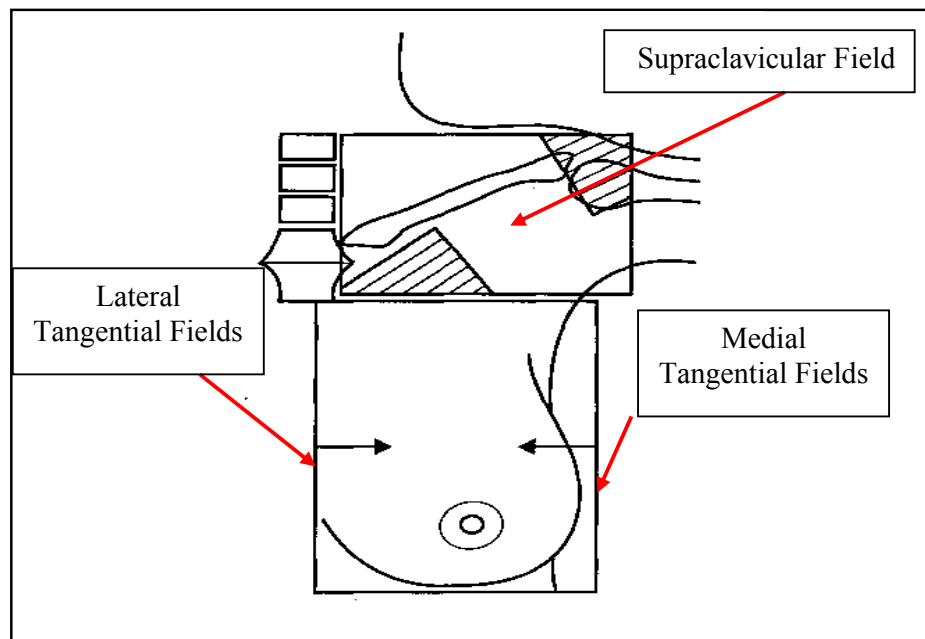


Figure 1.7: Anterior view for three-field technique. (Dobbles *et al.*, 1999).

### 1.3.3 Matching the Tangential Fields with the Supraclavicular Field (SCF)

An overdose caused by divergence of the tangential beams into the supraclavicular field and of the supraclavicular beam into the tangential fields can exist just beneath the skin surface at the junction of the inferior border of the

supraclavicular field and the superior border of the tangential fields. (Bedwinek, 1981) The sharp beam of a linear accelerator and the "horns" at the edge of this beam produce a marked increase in dose beneath the matchline if these divergences are not corrected. This increased dose may result in severe matchline fibrosis or even rib fracture.

#### **1.3.4 Matching the Tangential Fields with the Internal Mammary Field**

When an internal mammary field is required, the match between it and the medial tangential field can be a problem if there is a significant amount of breast tissue beneath the matchline. In this situation, underdose areas can exist (Figure 1.8A). The effect may be negligible if the breast tissue beneath this matchline is thin (Figure 1.8B), or it can be avoided by not using a separate internal mammary field (Figure 1.8C). In the latter case, the internal mammary nodes must be included in the tangential beams (as determined by CT scan or radionuclide scintigraphy). Usually this can be achieved by moving the medial tangential field border 3 to 5 cm across the midline. The portal films should be inspected carefully to ensure that an excessive amount of lung or heart is not being irradiated. There is no good solution to this matchline problem in large-chested women who also have a significant amount of breast tissue beneath the matchline of the tangential and internal mammary fields. Woudstra and van der Werf, (1987) described a technique using an oblique incidence of the internal mammary portal to match the orientation of the adjacent medial tangential portal; this results in a more homogeneous dose distribution at the junction of the two fields.

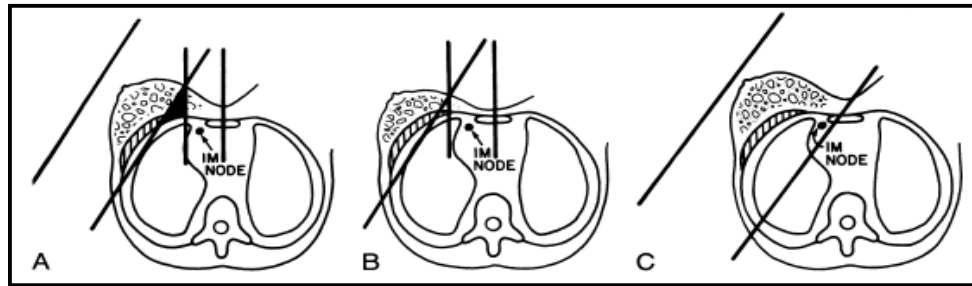


Figure 1.8: Diagrams showing several relationships between internal mammary and tangential fields. (A) A significant cold region exists if the internal mammary (IM) tangential matchline overlies a large amount of breast tissue. (B) The cold area may be negligible if the breast tissue beneath the matchline is thin. (C) The lack of a separate IM field can result in irradiation of an excessive volume of lung, particularly in large-chested patients. (Bedwinek, 1981)

#### 1.4 Research Objectives

The principal objectives of this research can be summarized in the following points

- 1) To examine different types of high-energy dosimeters such as TLD, films, and Si diode during breast cancer radiotherapy.
- 2) To compare different dosimetric techniques for investigating underdose and overdose in radiotherapy treatment planning.
- 3) To compare breast irradiation techniques in terms of reproducibility and accuracy.
- 4) To investigate the entrance and exit doses in vivo in breast radiotherapy with a 6 MV photon beam.
- 5) To investigate the dose for contralateral breast during radiotherapy treatment.

The local radiotherapy departments in Malaysia current situation is that they are using some breast irradiation techniques without research done for dose measurement for the matchline dose, tumour dose, and organ at risk (Contralateral Breast).

## **1.5 Structure of this Thesis**

This thesis contains seven chapters having the common theme, dose measurements in problematic treatment fields in breast cancer radiotherapy. Chapter 1 provides background information on external breast radiation therapy, spread of lymphatic routes of breast anatomy, description of treatment fields, and the main objectives of this research.

A literature review on the dose measurements in problematic breast cancer radiotherapy and organs at risk is given in chapter 2. It is divided into four broad categories: i) Matchline of supraclavicular and tangential breast fields techniques, ii) Lung and heart dose during breast radiotherapy, iii) Entrance and exit dose, and iv) Contralateral breast dose. Chapter 3 describes the instrumentation utilized in this research. There were two main categories of instruments used, namely the detectors and the TLD reader with the ancillary equipments. The detectors employed included the TLDs which are described in greater detail whereas other detector types such as n-type Si semiconductor diodes and the film dosimeters are also touched upon. The central piece of material for the research is the phantom. Three types of phantoms were described, namely the solid water phantom, perspex phantom and the heterogeneous phantom. The perspex plays a major role in this research. As a treatise in instrumentation, the simulator and linear accelerator (LINAC) are also described.

Validation of the experimental work for dose calculations and measurements is provided in the following four chapters. Chapter 4 presents the three field technique in post-mastectomy chest wall radiotherapy involving supraclavicular nodes. Four different techniques (overlap, couch rotating, 5 mm gap asymmetric jaw, and 5 mm gap symmetrical field) were examined and experiments carried out to compare the calculation results with the measurements. The dosimeters' response

behaviors were studied. For LiF:Mg;Ti TLD, the characterization included seven parameters with respect to reproducibility, linearity, field size, angular dependence, effect of wedge, dose rate dependence and percentage depth dose. In the case of film, only the calibration curve and the percentage depth dose curve were studied.

In chapter 5 the entrance and exit dose for lateral, medial (tangential fields) and three fields were investigated. 6 MV photon beam for breast radiotherapy now employed was used with TLDs and also the n-type VeriDose Diode for patient dosimetry. The latter is further elaborated on dose perturbation, calibration for the entrance and exit doses and temperature dependence. An observation on the parameters affecting measurements was also presented.

Chapter 6 presents a comparative study of the contralateral breast in phantom and patient dosimetry. Finally, chapter 7 concludes the thesis providing a summary of the major results and potential avenues for future work.

## CHAPTER 2

### LITERATURE REVIEW

#### 2.1 Matchline of Supraclavicular and Tangential Breast Fields Techniques

The treatment of the breast and adjacent lymph nodes requires a complicated irradiation technique due to the irregular target volume that lies close to the critical organs. Frequently, a technique that utilizes three fields is used. Typically this consists of the application of two opposite tangential fields for breast, chest wall, and ipsilateral internal mammary lymph nodes irradiation. A third anterior field is applied to irradiate supraclavicular and axilla lymph nodes. Overdosage as a result of an overlap of the supraclavicular, axillary and tangential breast fields can cause unacceptable fibrosis and cosmetic impairment (Harris *et al.*, 1979; Clarke *et al.*, 1983; and Pezner *et al.*, 1985). An underdosage area as a result of a gap can contribute to tumour recurrence. It is therefore important that tangential breast fields and supraclavicular fields are matched as precisely as possible. A further complication of the tangential field treatment is the location of internal mammary nodes over an oblique plane close to the sternum. While irradiating the internal mammary nodes a low dose should be maintained to underlying lung tissue. Several ways have been proposed to solve these problems (Svensson *et al.*, 1980; Siddon *et al.*, 1980; Siddon *et al.*, 1983; Podgorsak *et al.*, 1984; Lebesque, 1986; and Litcher *et al.*, 1986). To avoid the overlap from beam divergence and to carefully match the adjacent fields, Podgorsak *et al.*, (1984) suggested the use of half beam blocks. Many techniques have been proposed to achieve uniform dose distributions across the junction of abutting tangential and supraclavicular fields. Most of these approaches

attempt to avoid over- or underdosage through a combination of couch rotation, collimator rotation, half beam blocks, asymmetric jaws or beam splitters.

Svensson *et al.*, (1980) were the first to describe an isocentric technique which produced a geometric alignment between the supraclavicular field (SCF) and tangential breast fields using a hanging corner block on the superior border of the tangential fields and modified the beam divergence by rotating the couch. Mounted corner was replaced of hanging block by (Siddon *et al.*, 1983).

Hunt *et al.* (1987) compared the dose distributions for different treatment techniques. These authors analyzed the influence of various geometrical parameters on the dose distribution in the match region. In all these techniques, however, no gaps or overlaps are assumed between adjacent fields. In a previous study Holmberg *et al.*, (1994) determined *in vivo* the accuracy of field matching in breast cancer irradiation using an electronic portal imaging device assessed the four field edge positions in the cranial match plane of tangential breast fields and supraclavicular-axillary fields. The mean gap/overlap of the four fields for individual patients during each treatment session was +0.5 mm indicating that no systematic gap or overlap was observed. The uncertainty in the position of the tangential and supraclavicular fields with respect to the match plane ranged from 3.1 to 5.1 mm (1 SD) for the individual patients. Therefore, it can be expected that these set-up uncertainties will cause dose fluctuations across the abutment of matching fields. The effect of set-up uncertainties on the dose across the junction of matching craniospinal fields in the treatment of medulloblastoma has been investigated by Holupka *et al.*, (1993). Only limited information is available, however, for such a dose perturbation during breast treatment (Marshall, 1993). Therefore, Idzes *et al.* (1998) evaluated the dose distribution in the match region when an optimal match is achieved and in cases

when gaps and overlaps occur between adjacent fields as a result of set-up uncertainties.

The divergence of the tangential fields into the SCF and vice versa can cause over dosage which may result in severe matchline fibrosis or even rib fracture (Perez and Brady, 1997). On the other hand, under dosage can result from a gap in between tangential fields and the SCF (Idzes *et al.*, 1998) and it could increase the recurrence rate.

## **2.2 Lung and Heart Dose during breast Radiotherapy**

Breast cancer radiotherapy patients usually receive radiotherapy to the breast and chest wall as part of their treatment because parts of the anterior lung will be included in the tangential radiation fields. The aim of the treatment is to deliver a uniform dose to the target volume (breast with or without the regional nodes) while sparing as much as possible the adjacent normal tissue. While such irradiation does not cause a clinically relevant problem, it is sometimes accompanied with clinically significant pneumonitis, particularly in patients previously treated with chemotherapy (Lingos *et al.*, 1991; Mah *et al.*, 1994).

The treatment techniques practiced in most departments have undergone evolution in line with the advances in technology. Dose comparison studies of modern techniques with those practiced in the earlier studies indicate a reduction in cardiac and lung dose and volume, predicting a decreased risk of cardiac and lung morbidity as a result (Price *et al.*, 1990; Host *et al.*, 1986; Fuller *et al.*, 1992). A variety of methods have been proposed to aid in the reduction of the volume of lung and heart encompassed in the target volume. These include modified electron/photon field arrangements (Hurkmans *et al.*, 2000), patients suspending their breathing

during treatment (Lu *et al.*; 2000), the practice of setting a maximum acceptable lung volume (Dobbs, 2000), and the ipsilateral arm raised in an optimum position forcing the breast anteriorly away from the lung (Canney *et al.*; 1999).

The primary indicator suggested as a guide to the lung volume included within the treatment volume is the central lung distance (CLD) (Lirette *et al.*, 1995 and Das *et al.*, 1998). This is the distance between the posterior field edge and the anterior edge of the lung at the field central axis plane. Alternative indicators of the lung/heart volume can be derived from portal images of the tangential fields or from CT scans of the target volume acquired using either a simulator CT (Mallik *et al.*, 1995) or a CT simulator.

Dose-volume analysis for three-dimensional (3D) CT patient data were studied by evaluation of the tangential treatment technique (Fuller *et al.*, 1992; Gagliardi *et al.*, 1996; Gyenes *et al.*, 1997; Gagliardi *et al.*, 1998; Das *et al.*, 1998; and Nixon *et al.*, 1998). In modern techniques including the locoregional lymph nodes in the target volume a few detailed information is available about cardiac doses (Pakisch *et al.*, 1991 and Jansson *et al.*, 1998).

Pakisch *et al.* (1991) calculated dose-volume histograms of the lungs and heart for treatment techniques including the lymph nodes in the target volume. However, they did not outline the target volume, so no information about target coverage was available. Jansson *et al.* (1998) presented data about heart and lung doses and target coverage, but the new technique which they studied can only be employed on an Medium Mammary 22 or Medium Mammary 50 Racetrack microtron of which only a few exist in the world. They compared their new technique with a tangential irradiation technique, which has the disadvantage that

generally a considerable part of the contralateral breast has to be included to obtain adequate target coverage.

A correlation between CLD and irradiated lung volume has been studied by Bornstein *et al.*, (1990) and Carter *et al.*, (1997). Bornstein *et al.*, (1990) described a technique in which the collimator is rotated parallel to the chest wall such that the deep field edge is defined by the collimator. In the technique utilized by Carter *et al.*, (1997) study technique, the collimator is not rotated and the deep field edge is defined by a block, which is generally designed to follow the contour of the chest wall. In the technique used by Bornstein *et al.*, (1990), the thickness of the lung shadow near the cephalad and caudal field edges are likely to be less than at the lung shadow at the central axis, owing to the curvature of the chest. Bornstein *et al.*, (1990) reported a mean of 90% prediction interval to involve  $\pm 7\%$  of ipsilateral lung volume. On the other hand, Carter *et al.*, (1997) reported a  $\pm 5\%$  variability of ipsilateral lung volume. Van Tienhoven *et al.*, (1991) have studied the impact of variabilities on irradiated lung. He reported that respiratory movement has minimal influence on treatment volume. Similarly, Carter *et al.*, (1997) suggested that typical variations in treatment setup have a small impact on irradiated lung volume.

It has been shown in previous studies that breathing suitability techniques can be used to reduce the radiation to heart and lung volumes, originally by exploiting lung inflation to reduce the amount of lung tissue in the radiation fields and spatially separate the heart from the target. Recently, Pedersen *et al.*, (2004) and Korreman *et al.*, (2005) have shown in two CT-studies that both voluntary deep inspiration breath-hold and free breathing end-inspiration gating can provide lung and heart dose reductions. Corresponding relative cardio-pulmonary normal tissue complication probability (NTCP) reductions were reported to be of the order of 85% for

pneumonitis and 95% for cardiac mortality (Korreman *et al.*, 2006a). Both the dosimetric and complication probability effects were slightly larger with the deep inspiration breath-hold technique than with the inspiration gating technique, however these differences were not statistically significant.

Since January 2004, the free breathing end-inspiration gating technique implemented with the Real-Time Position Management (RPM)<sup>TM</sup> system has been in routine clinical use at Copenhagen University Hospital institution. Audio coaching is used for all patients to increase the inspiration level of breathing, and is individualized in a training session prior to the planning CT-scanning. A study by Korreman *et al.*, (2006b) was the first that reported dose distributions and predicted normal tissue toxicities for a population of patients treated with the free breathing inspiration gating technique for breast cancer.

### **2.3 Entrance and Exit Dose for Breast Treatment**

Human skin consists of three main layers: they are in alternation epidermis, basal layer and dermis. The epidermis is mostly composed of dead cells and their function is mainly for protection. The thickness of the epidermis varies at different sites of the human body: approximately 4–5 mg/cm<sup>2</sup> thick on head, neck, trunk and upper parts of limbs, 10-15 mg/cm<sup>2</sup> at the back of hands and feet, and 30–40 mg/cm<sup>2</sup> on the palm and soles (Keirim-Markus, 1991). The basal layer, located at the lowest part of epidermis, is the skin cell provider and is considered to be where the skin damage occurs while receiving a radiation dose (Hopewell, 1991; ICRP, 1991; ICRU, 1985).

Both the oncologist and medical physicist are interested to know the dose at this specified region as well as the dose beyond. These are important pieces of

information for avoiding unwanted skin complication and for the treatment of the lymphatic system at the depth of 0.5 mm (Kron *et al.*, 1993). However, the dose measurement of the basal layer is rather difficult and complicated owing to the fact that the thickness and composition of skin vary at different parts of the human body and at some sites the basal layer is even wavy and overlapped with capillary glomerules. Nevertheless, the basal layer in thinner skin, as in a human body, is flatter and nearly constantly thick; this makes the use of an ultra-thin dosimeter possible *in vivo*.

Measurements of skin dose and exit dose have been studied by various methods (Purdy, 1986; Rikner and Grussel, 1989; Thomas and Palmer, 1989; Rawlinson *et al.*, 1992; Kron *et al.*, 1993). Many types of detectors can be used for *in vivo* dosimetry (ICRU, 1976; Mckinlay, 1981; Rikner and Grussel, 1987); nevertheless, TLD and semiconductors are the most commonly used. A comparison of both detectors is worth being done in clinical practice of conventional treatments because the physical properties involved in the detection process are different and the calibration methodology requires some correction factors that are specific to each type of detector (Auket, 1991). Based on these arguments, we intended to measure entrance and exit doses with both dosimeters for breast patients treated isocentrically with external photon beam therapy. This feasibility study is aimed at investigating the calibration methodology and comparing the overall precision in the dosimetric data resulting from both dosimeters placed simultaneously on patients.

Most commercially available semiconductor detectors are designed to measure the dose at a certain depth in tissue as entrance dose measurements (Heukelom *et al.*, 1991). A build-up cap usually covered these semiconductor

detectors to take the active measurement point to a depth of 0.5 to 2.0 cm (Rikner *et al.*, 1987; Nilsson *et al.*, 1988).

Direct entrance dose measurement method in patients during dose delivery is still one of the best methods in use in terms of reliability. Radiotherapy departments can detect discrepancies on incidence dose and finally the target dose. In vivo monitoring thus forms a part of quality assurance programs to optimize treatment strategy. However the financial burden and the complexity of in vivo procedures as well as the perturbation effects of the dosimeters in the irradiated fields are the major obstacles toward implementing full-strength entrance dose measurement programs. A new, simplified, convenient, and reliable technique is needed to be developed. There exists now a technique using LiF TLDs without buildup cap (Banjade *et al.*, 2003) to measure the entrance dose in a patient undergoing radiotherapy which might prove to be beneficial.

## **2.4 Contralateral Breast Dose during Breast Treatment**

Many studies have been done in regard to contralateral breast cancer (CBC). The researchers concentrate their studies into two main areas, the risk of contralateral breast (CB) and how to reduce the dose to the non-affected area.

### **2.4.1 Contralateral Breast at Risk**

Regarding who is at risk, the only factor that has shown a link to increased CBC to radiotherapy is age and family history. Boice *et al.* (1992) examined the effect that the patient's age has in the risk of developing second malignancies after radiation therapy treatment. The study concluded the relative overall increase in risk of CBC after the treatment for the primary target by radiation was 1.19. It was also

found that the relative risk was 1.59 for patients under the age of 45 at the time of the treatment and this increased to 1.85 for 10 year survivors who were under the age of 45 at the time of the treatment.

The risk factors of CBC have been reasonably consistent in incriminating family history and age at diagnosis of the first breast cancer (Bernstein *et al.*, 1992; Chen *et al.*, 1999; Harvey and Brinton, 1985; Hemminki and Vaittinen, 1999; Prior and Waterhouse, 1978). Because early age of onset is a strong risk factor, the relative risk of CBC compared to unilateral disease decreases with age (Gajalakshimi *et al.*, 1998; Harvey and Brinton, 1985; Prior and Waterhouse, 1978). The time interval between the first and the second breast cancer has been considered in some earlier studies and the risk has been highest in the first year of follow-up (Horn *et al.*, 1987; Prior and Waterhouse, 1978). The data reported by Vaittinen *et al.*, (2000) was agreed but the magnitude of effect was relatively small, with a relative risk of 1.28. The data on the effects of reproductive factors have been contradictory. The well-established risk factors of unilateral breast cancer, late age at first childbirth and low parity, are not established risk factors of contralateral breast cancer: some studies exhibit effects, others exhibit no effects or exhibit even opposite effects, as reviewed by (Chen *et al.*, 1999). Vaittinen *et al.*, (2000) reported an exhibited a modest effect of parity and age at first childbirth.

Gao *et al.* (2003) showed a relative risk of 1.32 for patients under 45 as well as a risk of 1.15 for patients over 55. These studies all suggest that the younger the patient was at the time of the radiation treatment, then the greater the risk that they may develop a secondary malignancy in CB. However, Obedian *et al.* (2000) found 15 year follow up rates for patients under 45 of 10% for conservative surgery followed by radiotherapy and 7% for patients undergoing radical mastectomy. It was

concluded in the study that the increase was not statistically significant. Although the direct correlation between second malignancies and radiotherapy is not fully known and still under debate, it is a prudent practice to minimize any factor that may cause an increase in risk.

#### **2.4.2 Minimizing Contralateral Breast Dose**

Fraass *et al.* (1985) demonstrated, through various techniques, different methods to reduce the radiation peripheral dose during treatment. One of these techniques dealt with removing the wedge from medial tangential field. Other studies also show that the majority of the CB dose is produced by the medial tangent beam, whereas, the dose from the lateral tangent beam has to transverse through several centimeters of tissue before it reaches the CB.

Tercilla *et al.* (1989) studied CB dose using half beam blocks and isocentric treatment techniques for 15 patients treated with primary breast radiotherapy using a Co-60 unit. They observed that the isocentric treatment technique is a simple solution for reduction of CB dose. On the other hand, Kelley *et al.* (1996) reported a study of four different techniques with a 6 MV linac beam. Using the Rando phantom and TLDs, they set up the beam arrangements as half beam with custom blocks, half beam using asymmetric collimator jaws, half beam using asymmetric collimator jaws with custom blocks, and isocentric technique with non divergent posterior border. They observed the highest dose for the medial field with a wedge and the lowest with asymmetric jaws and no medial wedge or block.

Weides *et al.* (1995) and Warlick *et al.* (1997) evaluated the CB dose during breast irradiation using dynamic and regular wedges, with the development of the dynamic wedge and its application in breast conservation treatments, the absorbed

dose to the CB is reduced on average by 40%. These doses are only slightly higher than treatment with an open field.

Bhatnagar *et al.* (2004) reported comparison of IMRT and conventional tangential field technique with wedges. They observed the CB dose of  $7.24 \pm 2.35\%$  of the primary breast dose (5000 cGy) in IMRT and  $9.24 \pm 2.04\%$  of the primary dose using the conventional tangential field technique. This shows a 20% reduction on dose to the CB dose (362 cGy IMRT and 462 cGy conventional).

Muller-Runkel *et al.* (1990), Sohn *et al.* (1999), and Goffman *et al.* (2004) utilized in various methods lead shielding to reduce the dose to the CB. All showed a reduced dose in their studies. These reductions ranged from one third to one half of the original measured dose to the CB. Chougule *et al.* (2007) used a Co-60 unit to measure the dose to the CB for numerous patients. It was concluded that the dose generated by the medial tangential field was almost twice as much as the lateral tangential field. It was also postulated that a considerable amount of the dose from the lateral field was due to internal scatter and the dose from the medial field was primarily attributed to the scatter from the collimator.

## CHAPTER 3

### GENERAL INSTRUMENTATION

#### 3.1 Introduction

Proper and precise delivery of radiation consists of a complex series of events. These events must be controlled and monitored to ensure that the prescribed dose is given as accurately as possible in order for the treatment to be successful. The first control is established before the patient is even treated. It also involves the radiation delivery unit, the linear accelerator (linac). It must undergo extensive quality assurance tests. These tests keep the linac functioning within precise parameters that have been set up.

The treatment of a cancer patient begins from a visit to the radiation oncologist. After a series of tests, the images (Simulator, CT, MRI, etc.) are captured for the purpose of diagnosis. The oncologist determines the stage of progress of the cancer and a treatment plan; chemotherapy, surgery, radiation, or any combination that may be administered. When radiation is the method chosen, the doctor gives a prescribed dose to treat the patient. This treatment may be a means to a cure or palliative.

Once the method of treatment and dose are prescribed, the images from the patient's CT scan are used to determine the contours of the critical organs and the cancerous growth(s). This is done using the treatment planning system (TPS) that corresponds to each individual linac. The limiting factor for the delivery of radiation is the consideration of the normal tissue surrounding the diseased area. Normal tissue can only be exposed to so much radiation dose before it cannot function properly.